



Tunable mode convertor based on fiber Bragg grating inscribed in graded-index nine-mode fiber

RUI LIU,^{1,2} ZHIYONG BAI,^{1,2,*}  JIAYAN CHEN,^{1,2} ZILUN LUO,^{1,2} LUPING WU,^{1,2} JIANJUN RAN,^{1,2} CHANGRUI LIAO,^{1,2}  JUN HE,^{1,2}  XIAOYU WENG,¹  LIWEI LIU,¹ JUNLE QU,¹ AND YIPING WANG^{1,2} 

¹Key Laboratory of Optoelectronic Devices and Systems of Ministry of Education and Guangdong Province, College of Physics and Optoelectronic Engineering, Shenzhen University, Shenzhen 518060, China

²Shenzhen Key Laboratory of Photonic Devices and Sensing Systems for Internet of Things, Guangdong and Hong Kong Joint Research Centre for Optical Fibre Sensors, Shenzhen University, Shenzhen 518060, China

*baizhiyong@szu.edu.cn

Received 10 February 2023; revised 25 March 2023; accepted 28 March 2023; posted 28 March 2023; published 17 April 2023

A tunable mode convertor is experimentally demonstrated based on a fiber Bragg grating (FBG), which is fabricated in a graded-index nine-mode fiber by using a femtosecond laser. Nine linearly polarized (LP) modes were excited and the coupling efficiency of them can reach 90%. By adjusting the polarization controller, the ± 1 st-, ± 2 nd-, ± 3 rd-, and ± 4 th-order orbital angular momentum (OAM) modes were excited, which means the OAM tuning of $0-\pm 1\hbar$, $0-\pm 2\hbar$, $0-\pm 3\hbar$, and $0-\pm 4\hbar$ were achieved. LP_{21}/LP_{02} , LP_{31}/LP_{12} , $LP_{41}/LP_{22}/LP_{03}$ modes were successfully tuned at 1556.00 nm, 1555.10 nm, and 1554.25 nm by twisting the FBG, respectively. Moreover, combined with polarization and torsion control, the tuning between 0th- and -2 nd-order OAM has been realized, which is converted from the tuning between LP_{02} and LP_{21} . By using this method, the OAM tuning of $\pm 1-\pm 3\hbar$ and $\pm 4-0-\pm 2\hbar$ may be further realized theoretically. © 2023 Optica Publishing Group

<https://doi.org/10.1364/OL.487336>

In 1992, Allen *et al.* presented the orbital angular momentum (OAM) in vortex beams [1], which have been extensively investigated and applied in the fields of complex optical manipulation [2], super-resolution microscopy [3], high-sensitivity sensing [4], and large-capacity communication [5]. These beams are characterized by the Hilbert factor $\exp(il\varphi)$ and carry OAM equivalent to $l\hbar$ per photon, where l is the topological charge and φ is the azimuth angle. With the rapid development of OAM, the tunability of the topological charge becomes increasingly critical. In the fields of sensing, optical manipulation, and optical communication, different l means different sensing sensitivities [6], different optical torques [7], and signal transmission and coding in different channels [8], respectively. Numerous methods and technologies have been proposed. Spatial light modulators [9] are mature in technology, excellent in flexibility, but are not compatible with the optical fiber communication system and are unstable due to their large volume and high insertion loss. To avoid these problems, the generation methods based on all-fiber have been proposed and developed.

In 2016, Zhang *et al.* presented a tunable fiber laser with an acousto-optic fiber grating and realized an OAM tuning of $0-\pm 1\hbar$ [10]. In the following year, Zhao *et al.* proposed a mode convertor based on two cascaded long period fiber gratings (LPFGs) reaching the OAM tuning of $0-\pm 2\hbar$ [11]. Gao *et al.* obtained the OAM tuning of $0-\pm 2\hbar$ based on a strong modulated LPFG [12]. In 2020, our group proposed an OAM generator based on an FBG, and by controlling the offset distance, obtained an OAM tuning of $0-\pm 2\hbar$ [13]. In the same year, Yang *et al.* reported $0-\pm 3\hbar$ OAM tuning based on a tilted FBG [14]. However, the acousto-optic fiber grating can tune the grating pitch flexibly but requires complex systems. The fiber coupler and the LPFG reduce the complexity but can only realize transmission-type OAM conversion. Controlling the offset distance also requires precise alignment. An FBG-based convertor is simple and can realize the reflected OAM mode, with wide applications in fiber lasers [14,15]. To our knowledge, the highest order OAM tuning based on an FBG is $0-\pm 3\hbar$, and the mode tuning between linearly polarized (LP) modes and OAM tuning between non-zero orders has not been implemented.

In this Letter, we report a tunable mode converter based on the FBG inscribed in a graded-index nine-mode fiber. By adjusting the polarization controller, we achieve an OAM tuning of $0-\pm 1\hbar$, $0-\pm 2\hbar$, $0-\pm 3\hbar$, and $0-\pm 4\hbar$. Additionally, we obtain the mode tuning of LP_{21}/LP_{02} , LP_{31}/LP_{12} , $LP_{41}/LP_{22}/LP_{03}$ at 1556.00 nm, 1555.10 nm, and 1554.25 nm, respectively, by twisting the FBG. Moreover, combining the OAM mode conversion, we successfully obtained the OAM tuning of 0 to $-2\hbar$ converted from the mode tuning between LP_{02} and LP_{21} .

The graded-index nine-mode fiber (YOFC) used in our experiment has core and cladding diameters of 33 μm and 125 μm , respectively, and can theoretically support LP_{01} , LP_{11} , LP_{21} , LP_{02} , LP_{31} , LP_{12} , LP_{41} , LP_{22} , and LP_{03} modes long-distance transmission. A femtosecond laser with a wavelength of 513 nm, a pulse width of 290 fs, and a repetition rate of 200 kHz was focused by a 100 \times Leica oil-immersion objective with a numerical aperture (N.A.) of 1.25, and a refractive index matching oil ($n = 1.4587$) was used to eliminate aberration induced by the cylindrical geometry of the fiber. As shown in Fig. 1, the FBG

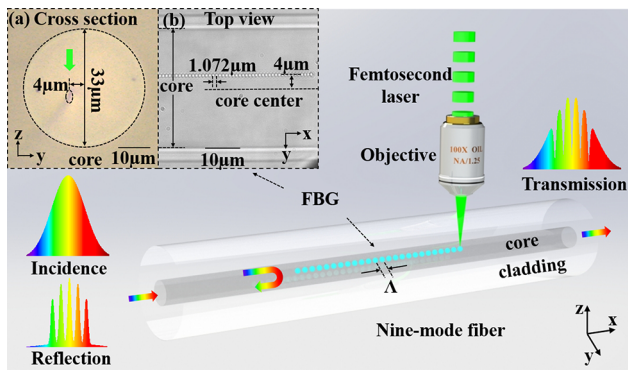


Fig. 1. Schematic of the FBG fabricated by femtosecond laser on a graded-index nine-mode fiber. (a) Cross section and (b) top view microscopy image of an FBG with off-axis displacement $D = 4 \mu\text{m}$.

is fabricated by femtosecond laser direct writing, and the process is as follows: first, the nine-mode fiber was clamped by a pair of fiber holders mounted on a three-dimensional air-bearing translation stage, and the femtosecond laser was focused into the center of the fiber core. The axial direction of the fiber and the incident direction of laser are parallel to the x axis and the z axis of the translation stage, respectively. Second, the fiber was moved along the y axis so that the focus of the laser has an off-axis displacement D from the center of the fiber core, and the position is the starting point of the FBG. Finally, the translation stage was moved along the x axis at a speed matched to the repetition rate of the femtosecond laser to periodically modulate the fiber core with a single pulse energy of 24 nJ. The cross section and the top view microscopy images of the fabricated FBG are shown in Figs. 1(a) and 1(b), respectively. According to the phase-matching condition, the FBG with a pitch of $1.072 \mu\text{m}$ is coupled in the conventional band of optical communication.

To determine the effect of D on mode coupling, four FBGs S1–S4 with the same grating pitch $\Lambda = 1.072 \mu\text{m}$, length $L = 3 \text{ mm}$ were fabricated with the same single pulse energy 24 nJ. As shown by the top-view microscopy images in Figs. 2(a1)–2(a4), D of S1–S4 was increased from $0 \mu\text{m}$ to $6 \mu\text{m}$ with a step of $2 \mu\text{m}$. The corresponding transmission spectra of S1–S4 were measured by using a broadband light source and a spectrometer in real time during the preparation of the FBGs, and the spectra are shown in Figs. 2(b1)–2(b4). From the long wavelength to the short wavelength direction, as shown in Fig. 2(b), the odd resonant dips are marked as o_1, o_2, o_3, \dots , and the even resonant dips are marked as e_1, e_2, e_3, \dots . In the case of FBG S1 with $D = 0 \mu\text{m}$, almost only the odd resonant dips were excited. Among the o_1 – o_3 and the e_1 – e_3 , the e_1 with minimum coupling efficiency is only -1.465 dB . When $D = 2 \mu\text{m}$, the even resonant dips were excited, with e_1 having the minimum coupling efficiency of -5.689 dB . As D is increased to $4 \mu\text{m}$, the coupling efficiency of each resonant dip is relatively close and the minimum one e_1 can reach -9.265 dB . However, when $D = 6 \mu\text{m}$, the coupling efficiency of each resonant dip decreased and the minimum one e_2 is only -2.738 dB . Based on our analysis, we chose the FBG with $D = 4 \mu\text{m}$ for subsequent experimental tests because its coupling efficiency of each dip is closer and each of them is up to -9.265 dB .

We designed and setup a system to detect the mode intensity distribution, interference patterns, and reflection spectrum of the FBG. To ensure normal incidence of the beam, we have

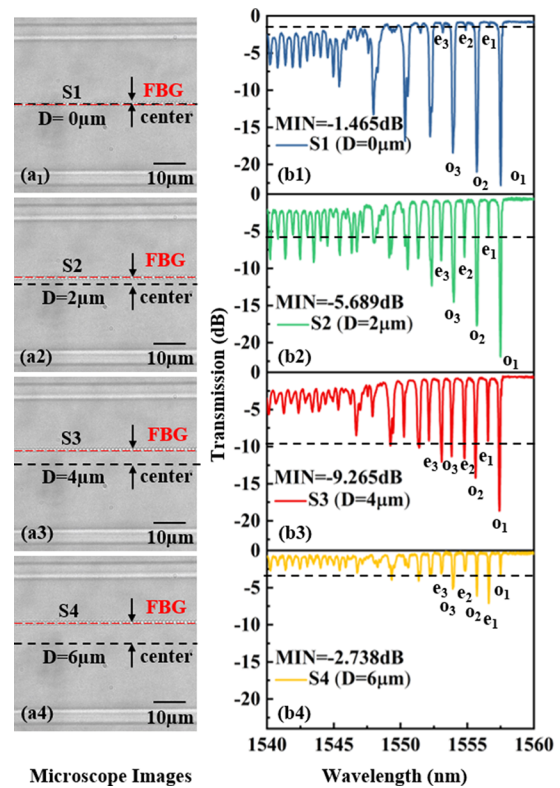


Fig. 2. Microscopy images and transmission spectra of FBGs S1–S4 located at different positions with off-axis displacement D of $0 \mu\text{m}$, $2 \mu\text{m}$, $4 \mu\text{m}$, and $6 \mu\text{m}$: (a) top view microscopy images and (b) corresponding transmission spectra of S1–S4.

calibrated the detecting system by applying the principle of optical path reversibility before testing. As shown in Fig. 3(a), the light beam from the tunable laser source was collimated by a $40\times$ objective lens (Obj_1), then divided into two paths by a beam splitter 1 (BS_1) shown by the red line in the figure. One path was used as the reference beam and the other path was normally incident into the FBG to excite the reflected mode. The polarization controller (PC) located before the FBG is used to generate the OAM mode by changing the relative amplitudes and phases of the coupled modes. In addition, the beam reflected by the FBG, as shown by the blue line in the figure, was divided into two paths by BS_3 . One of them was collimated by Obj_3 and incident onto the power meter. The other one was combined and coaxially interfered with the reference beam at BS_4 , as shown by the green line in the figure. In addition, the neutral density filter (NDF) located between BS_1 and BS_4 was used to match the intensity of the two beams to improve the contrast of the interference fringes. The tunable laser performed wavelength scanning of the FBG, and then the power of each wavelength was recorded by the power meter to obtain the reflection spectrum. A CCD was used to detect the mode intensity distribution and the interference pattern.

The reflection spectrum of the FBG is shown in Fig. 3(b). Transmission loss and coupling loss caused the reflection spectrum to lack some high-order modes relative to the transmission spectrum. The resonant peaks o_1, e_1, o_2, e_2, o_3 were located at the wavelengths of 1557.75 nm , 1556.87 nm , 1555.97 nm , 1555.09 nm , and 1554.24 nm , respectively. According to the reflection spectrum, we adjusted the output wavelength of the

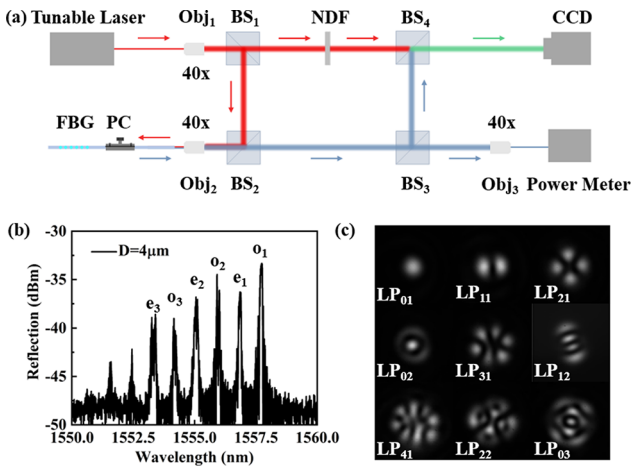


Fig. 3. (a) Experimental setup for detecting (b) reflection spectrum and (c) mode intensity distribution of the FBG.

tunable laser to the wavelength of each resonant peak in turn. As shown in Fig. 3(c), the LP₀₁ mode was found at the o₁, the LP₁₁ modes was found at the e₁, the LP₂₁ and LP₀₂ were found around the o₂, the LP₃₁ and LP₁₂ modes were found around the e₂, and the LP₄₁, LP₂₂, and LP₀₃ modes were found around the o₃. Because the resonant wavelengths of some modes were close to each other, the mode fields with smaller wavelength intervals were investigated. Figures 4(a1)–4(a5) and 4(b1)–4(b5) show the spectra of the above five peaks with the wavelength resolution of 0.02 nm and the mode intensity distribution at each wavelength within the spectra, respectively. Figure 4(a1) shows the spectrum in the range of 1557.6–1557.9 nm, and the corresponding mode belongs to LP₀₁, as shown in Fig. 4(b1). Figure 4(a2) shows the spectrum in the range of 1557.6–1557.9 nm, and the corresponding mode belongs to LP₁₁, as shown in Fig. 4(b2). In Fig. 4(a3), in the range of 1555.8–1556.1 nm, there are two peaks in the spectrum, and the corresponding modes belong to LP₂₁ and LP₀₂ at 1555.94 nm and 1556.0 nm, respectively. As for the Figs. 4(a4) and 4(b4), 4(a5) and 4(b5), there are two and three unobtrusive peaks, respectively, and the LP₃₁, LP₁₂, LP₄₁, LP₂₂, and LP₀₃ were located at 1555.10 nm, 1555.06 nm, 1554.25 nm, 1554.21 nm, and 1554.15 nm, respectively. The difference between the mode field distributions in Fig. 3(c) and

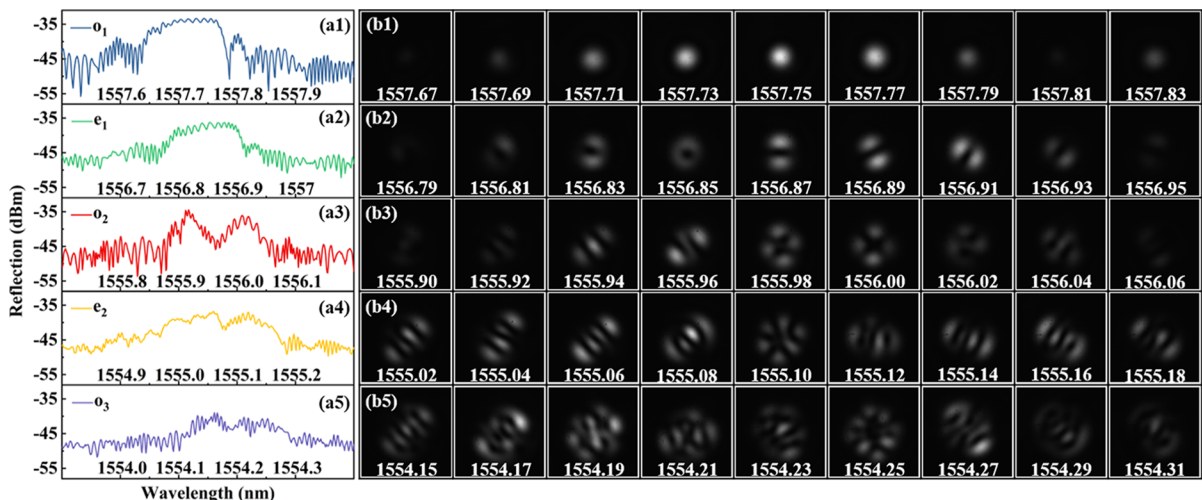


Fig. 4. (a1)–(a5) Local spectrum and (b1)–(b5) detailed mode intensity distribution of o₁, e₁, o₂, e₂, o₃, respectively.

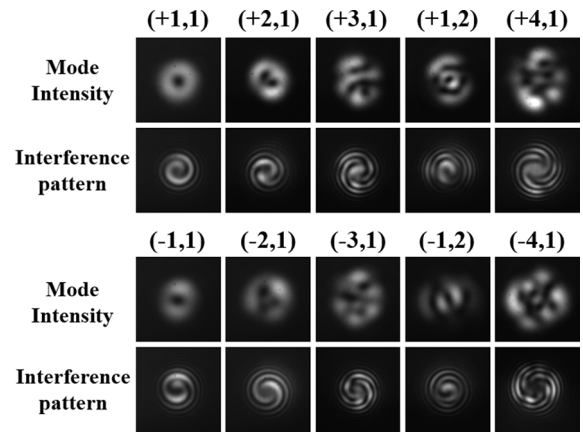


Fig. 5. Mode intensity distribution and the interference pattern of ± 1 st-, ± 2 nd-, ± 3 rd-, and ± 4 th-order OAM modes.

Fig. 4 is caused by the different polarization states of the two tests. As a result, we have successfully excited nine LP modes for long distance transmission in a graded-index nine-mode fiber, and studied the evolution law between adjacent modes.

To generate the OAM mode, we add a PC in front of the FBG. By adjusting the PC, the LP mode can be turned to the OAM mode. As the mode intensity distribution and interference pattern shown in Fig. 5, $(\pm 1, 1)$ represents the ± 1 st-OAM mode converted from the LP₁₁ mode, $(\pm 2, 1)$ represents the ± 2 nd-order OAM mode converted from the LP₂₁ mode, $(\pm 3, 1)$ represents the ± 3 rd-order OAM mode converted by the LP₃₁ mode, $(\pm 1, 2)$ represents the ± 1 st-order OAM mode converted by the LP₁₂ mode, and $(\pm 4, 1)$ represents the ± 4 th-order OAM mode converted by the LP₄₁ mode. In other words, it means the FBG we fabricated realized an OAM tuning of $0-\pm 1h$, $0-\pm 2h$, $0-\pm 3h$, and $0-\pm 4h$.

Since the resonant wavelength of some modes like LP₂₁ and LP₀₂ are close to each other, mode tuning can be achieved by adjusting external parameters like torsion. We twisted a 10-cm optical fiber region with the grating in the middle. As shown in the first line of Fig. 6, the reflection mode of LP₂₁ can be clearly observed when the wavelength of incident light is 1556.00 nm and the torsion angle is 0° and 10° . When the torsion angle reached $20^\circ-40^\circ$, the four-lobes mode intensity distribution within the LP₂₁ mode began to be connected. When the

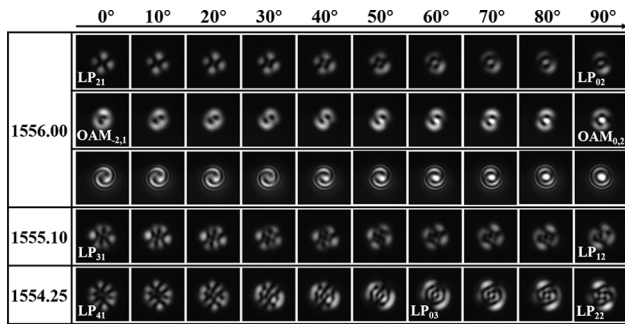


Fig. 6. Mode tuning with torsion angle from 0° to 90° at the wavelengths 1556.00 nm, 1555.10 nm, and 1554.20 nm.

torsion angle continued to increase to 50° , bright spots began to appear in the center of the mode intensity distribution. Until the torsion angle reached 90° , the reflection mode completely changed to LP_{02} . As shown in the fourth line of Fig. 6, when the wavelength of the incident light was 1555.10 nm, and the torsion angle was 0° , the reflection mode was LP_{31} . As the torsion angle increased gradually, the reflection mode gradually changed to LP_{12} when the torsion angle reached 90° . As shown in the fifth line in Fig. 6, the phenomenon was similar, when the wavelength of the incident light was 1554.25 nm, LP_{41} , LP_{22} , and LP_{03} modes appeared with the torsion angle of 0° , 60° , and 90° , respectively. Thus, it is proved that we realized LP mode tuning by twisting the FBG. By combining this tuning method with the generation of the OAM mode, the OAM tuning was realized in a new way. As shown in the second and the third lines in Fig. 6, with the torsion angle increasing, the mode intensity distribution was converted from the -2nd -order OAM mode $(-2,1)$ to the LP_{02} mode, which is also called 0th-order OAM mode $(0,2)$. Additionally, corresponding to the mode intensity distribution, the coaxial interference patterns also proved that the OAM tuning of 0 to $-2\hbar$ was achieved. It means precise OAM mode tunings were realized by calibrating the angles of the three-paddle fiber polarization controller and fiber rotator. Furthermore, because the modes LP_{31} , LP_{12} , LP_{41} , LP_{03} , and LP_{22} can convert to the $\pm 3\text{rd}$ -, $\pm 1\text{st}$ -, $\pm 4\text{th}$ -, 0th-, and $\pm 2\text{nd}$ -order OAM mode, respectively, the OAM tuning of $\pm 1 \sim \pm 3\hbar$, $\pm 4 \sim \pm 2\hbar$ can be achieved theoretically. However, due to the interference of the outer ring number of the mode field, it was difficult to observe whether $+1 \sim +3\hbar$ and $+4 \sim +2\hbar$ OAM tuning was realized.

In this work, a tunable OAM mode convertor has been demonstrated. The LP_{01} , LP_{11} , LP_{21} , LP_{02} , LP_{31} , LP_{12} , LP_{41} , LP_{22} , and LP_{03} modes were excited and the coupling efficiency of them can reach 90%. By controlling the polarization of the LP modes, the $\pm 1\text{st}$ -, $\pm 2\text{nd}$ -, $\pm 3\text{rd}$ -, and $\pm 4\text{th}$ -order OAM modes were

excited experimentally. Due to the similar resonant wavelengths, LP_{21}/LP_{02} , LP_{31}/LP_{12} , $LP_{41}/LP_{22}/LP_{03}$ were tuned at 1556.00 nm, 1555.10 nm, and 1554.25 nm by twisting the FBG, respectively. Furthermore, we achieved the important OAM tuning of 0 to $-2\hbar$ by a new method, which can realize the OAM tuning between non-zero orders. Additionally, the OAM tuning of $\pm 1 \sim \pm 3\hbar$ and $\pm 4 \sim 0 \sim \pm 2\hbar$ can be further realized theoretically. This convertor is capable of easy extension to other graded index fibers to generate the high order OAM mode and achieve tuning of OAM. Because of its easy design and fabrication process, it has a wide application in optical communication systems, as well as mode and wavelength division multiplexing.

Funding. National Natural Science Foundation of China (62275169); Natural Science Foundation of Guangdong Province (2022A1515010183); Shenzhen Science and Technology Program (ZDSYS20220606100405013).

Disclosures. The authors declare no conflicts of interest.

Data availability. Data underlying the results presented in this paper are not publicly available at this time but may be obtained from the authors upon reasonable request.

REFERENCES

1. L. Allen, M. W. Beijersbergen, R. J. Spreeuw, and J. P. Woerdman, *Phys. Rev. A: At., Mol., Opt. Phys.* **45**, 8185 (1992).
2. S.-Y. Huang, G.-L. Zhang, Q. Wang, M. Wang, C. Tu, Y. Li, and H.-T. Wang, *Optica* **8**, 1231 (2021).
3. L. Yan, P. Gregg, E. Karimi, A. Rubano, L. Marrucci, R. Boyd, and S. Ramachandran, *Optica* **2**, 900 (2015).
4. D. Deng, H. Zhao, J. Ni, Y. Li, and C.-W. Qiu, *Nanophotonics* **11**, 865 (2022).
5. N. Bozinovic, Y. Yue, Y. Ren, M. Tur, P. Kristensen, H. Huang, A. E. Willner, and S. Ramachandran, *Science* **340**, 1545 (2013).
6. A. Datta, A. Saha, and A. Shukla, *J. Opt. Soc. Am. A* **34**, 2034 (2017).
7. L. Zhu, M. Tang, H. Li, Y. Tai, and X. Li, *Nanophotonics* **10**, 2487 (2021).
8. J. Wang, J.-Y. Yang, I. M. Fazal, N. Ahmed, Y. Yan, H. Huang, Y. Ren, Y. Yue, S. Dolinar, M. Tur, and A. E. Willner, *Nat. Photonics* **6**, 488 (2012).
9. A. Forbes, A. Dudley, and M. McLaren, *Adv. Opt. Photonics* **8**, 200 (2016).
10. W. Zhang, K. Wei, L. Huang, D. Mao, B. Jiang, F. Gao, G. Zhang, T. Mei, and J. Zhao, *Opt. Express* **24**, 19278 (2016).
11. Y. Zhao, Y. Liu, C. Zhang, L. Zhang, G. Zheng, C. Mou, J. Wen, and T. Wang, *Opt. Lett.* **42**, 4708 (2017).
12. H. Wu, S. Gao, B. Huang, Y. Feng, X. Huang, W. Liu, and Z. Li, *Opt. Lett.* **42**, 5210 (2017).
13. Y. L. Li, Z. Y. Bai, Z. Liu, G. X. Zhu, K. M. Yang, J. Yu, J. Y. Chen, C. L. Fu, C. R. Liao, and Y. P. Wang, *Opt. Lett.* **45**, 6679 (2020).
14. K. Yang, Y.-g. Liu, Z. Wang, Y. Li, Y. Han, H.-w. Zhang, and B.-w. Mao, *Opt. Fiber Technol.* **55**, 102155 (2020).
15. Z. Huang, Q. Huang, A. Theodosiou, K. Kalli, S. Li, N. Chen, T. Chen, and C. Mou, *Opt. Laser Technol.* **143**, 107358 (2021).